JACS
JOURNAL OF THE AMERICAN CHEMICAL SOCIETY
Communication
pubs.acs.org/JACS

Size-Dependent Assemblies of Nanoparticle Mixtures in Thin Films

Joseph Kao,[†,⊥] Peter Bai,[†,⊥] J. Matthew Lucas,[‡] A. Paul Alivisatos,[†,§,∥] and Ting Xu*[,†,§,∥]

[†]Department of Materials Science & Engineering, University of California, Berkeley, California 94720, United States
[‡]Department of Mechanical Engineering, University of California, Berkeley, California 94720, United States
[§]Department of Chemistry, University of California, Berkeley, California 94720, United States
[∥]Materials Sciences Division, Lawrence Berkeley National Laboratory, Berkeley, California 94720, United States

Supporting Information

ABSTRACT: Hybrid nanoparticle (NP) arrays based on particles of different sizes and chemistries are highly desirable to obtain tunable properties for nanodevices. A simple approach to control the spatial organization of NP mixtures within supramolecular frameworks based on NP size has been developed. By varying the ratio of the NP size to the periodicity of the block-copolymer-based supramolecule, a range of hybrid NP assemblies in thin films, ranging from 1D chains to 2D lattices and 3D arrays and networks of NPs, can be readily generated.

Controlled coassemblies of nanoparticle (NP) mixtures with different chemical compositions can not only combine the properties of individual components but also lead to properties arising from the coupling effects between the NPs.[1−4] The fluorescence, optical absorption, and photocurrent of semiconductor NPs can be significantly affected by electromagnetic interactions in the vicinity of the metallic materials via the excitation of surface plasmon resonances.[5−9] Two-dimensional (2D) and three-dimensional (3D) binary NP superlattices have been obtained by coassembling monodispersed metal, semiconductor, and magnetic NPs of different sizes via controlled solvent evaporation. These studies led to NP solids with unique properties.[3,4,10] 2D arrays of metals or semiconductor NPs have been used to investigate their optical and/or electronic properties.[11−13] Functional hybrid nanocomposites can also be prepared by blending NPs with block copolymers (BCPs) or BCP-based supramolecules.[14−17] Enthalpically, NP ligands were chemically modified to tailor the NP−polymer interactions in order to control the spatial distribution of different types of NPs in BCP/NP blends.[18] Entropically, the penalty for deforming polymer chains upon NP incorporation depends on the ratio of the size of the NP to that of the polymer.[19] Simulations[19−21] and experimental studies[22] have revealed size-dependent spatial organization of different types of NPs in lamellar nanocomposites. NPs of different sizes can be selectively sequestered at the interface between two BCP lamellae or in the middle of the lamellar microdomains with good precision.[22] Many NP-based devices are based on thin films. However, directly extrapolating size-dependent, entropy-driven particle assemblies from the bulk to thin films of nanocomposites is not trivial because NPs tend to aggregate on the film surface to reduce entropic deformation of the polymer chains and lower the surface tension.[23−27] There is no straightforward route to direct coassemblies of different types of NPs in thin films to tailor the interparticle coupling and exchange phenomena.

We recently overcame the difficulties of surface aggregation of NPs in thin films using a BCP-based supramolecular approach.[28] Alkyl-ligand-capped NPs self-assemble into 3D hierarchical nanostructures in thin films where BCP cylindrical microdomains are oriented parallel to the surface. The formation of the observed 3D NP assemblies is entropically driven and can be attributed to the rigidity of the supramolecular comb block, which significantly enhances the entropic contribution from the NPs. The NPs selectively localized in the interstitial regions between BCP cylinders (Scheme 1) act as nanofillers to release the chain deformation of the rigid comb block. In the present work, the entropy-driven supramolecular approach was applied to obtain directed coassemblies of NP mixtures in thin films. Different NP assemblies ranging from 2D monolayers to 3D arrays/networks on the surface can be readily obtained simply by varying the NP size relative to the BCP periodicity. Furthermore, this approach can be applied to the coassembly of NP mixtures to obtain hybrid arrays of semiconductor and metallic NPs in thin films. The present studies open a new avenue for achieving structural control toward NP-based devices with different chemical compositions. It will also provide a powerful platform to test theoretical predictions of nanocomposite properties based on

Scheme 1. Schematic Drawing of the Distorted Hexagonal Lattice of PS(19 kDa)-*b*-P4VP(5.2 kDa)(PDP)$_{1.7}$ Thin Films after Solvent Annealing[a]

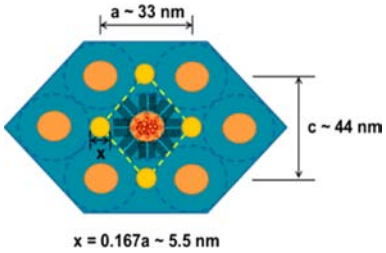

[a]The lattice constants a and c are 33 and 44 nm, respectively. The lateral dimension of each interstitial site is $x = 0.167a$ (i.e., 5.5 nm).

Received: November 1, 2012
Published: January 17, 2013

   dx.doi.org/10.1021/ja3107912 | J. Am. Chem. Soc. 2013, 135, 1680−1683

various coupling and exchange phenomena between the NP arrays.

The assembly of NPs upon blending with BCPs in thin films is determined by a combination of enthalpic and entropic contributions.[15] Qualitatively, the change in free energy upon incorporation of NPs can be described as

$$\Delta G = (\Delta H_{surface} + \Delta H_{ligand/polymer}) - T(\Delta S_{con} + \Delta S_{trans} + \Delta S_{geometric})$$

where $\Delta H_{surface}$ originates from the difference in the surface tensions of the components. Alkyl-ligand-capped NPs tend to segregate preferentially at the air/film interface to lower the surface tension.[23] To incorporate NPs into BCP microdomains in thin films, the NP ligands must interact favorably with at least one of the BCP blocks, providing the enthalpic driving force $\Delta H_{ligand/polymer}$.[15] Functional groups can be included in the NP ligands to strengthen the polymer−NP interactions in order to increase the energetic contribution from $\Delta H_{ligand/polymer}$.[29] ΔS_{con} refers to the change in conformational entropy of the polymer chains upon NP incorporation. Because of the geometric packing of the hexagonal lattice with cylindrical morphology, there is an additional entropic contribution, $\Delta S_{geometric}$, from the polymer chains surrounding the interstitial sites upon NP incorporation. This has been shown in homopolymer/BCP blends theoretically[30] and experimentally where homopolymers selectively localize in specific regions.[31,32] ΔS_{trans} accounts for the entropic contribution due to the number of physical arrangements of the NPs. The present studies mainly focused on the effects of various entropic contributions. The enthalpic contributions, $\Delta H_{ligand/air}$ and $\Delta H_{ligand/polymer}$, were kept constant. Entropically, the important parameters include the spring constant k (i.e., the rigidity of the polymer chain) and the d/a ratio, where d is the diameter of the particle (including the ligand shell) and a is the lateral periodicity of the supramolecule.

The BCP-based supramolecules, called "PS-*b*-P4VP(PDP)$_{1.7}$" [PS = polystyrene; P4VP = poly(4-vinylpyridine); PDP = 3-pentadecylphenol], were constructed by hydrogen bonding of PDP molecules to the 4VP groups in PS(19 kDa)-*b*-P4VP(5.2 kDa) at a PDP/4VP molar ratio of 1.7. Deforming the rigid P4VP(PDP)$_{1.7}$ chains should be entropically costly.[28] All of the NPs were passivated with alkyl ligands and preferentially solubilized within the P4VP(PDP)$_{1.7}$ matrix. Thin films of PS(19 kDa)-*b*-P4VP(5.2 kDa)(PDP)$_{1.7}$ supramolecular nanocomposites form a distorted hexagonal lattice with lattice constants $a \approx 33$ nm and $c \approx 44$ nm after solvent annealing (Scheme 1).[28] The lateral dimension of an interstitial site is $x = 0.167a$ (i.e., 5.5 nm). The d/a ratio was varied by using NPs of different sizes. The NP sizes were selected on the basis of the lattice constants of the cylindrical supramolecules. PbS NPs with overall sizes of 5.5, 7.4, and 9.3 nm; Au NPs with overall sizes of 5.7 and 7.4 nm; and PbSe NPs with an overall size of 9.0 nm were used. The overall particle size, d, reflects the sum of the NP core diameter and the ligand shell thickness. The methodology for calculating d and the d/a ratio is detailed in the Supporting Information (SI).

Figure 1a shows top-view and cross-sectional transmission electron microscopy (TEM) images of a ∼180 nm thin film of PS(19 kDa)-*b*-P4VP(5.2 kDa)(PDP)$_{1.7}$ blended with a 10 vol % loading of the 9.3 nm PbS NPs. The PbS NPs formed ordered arrays located at the air/polymer interface, one NP in width, conforming to the contours of the fingerprint-like

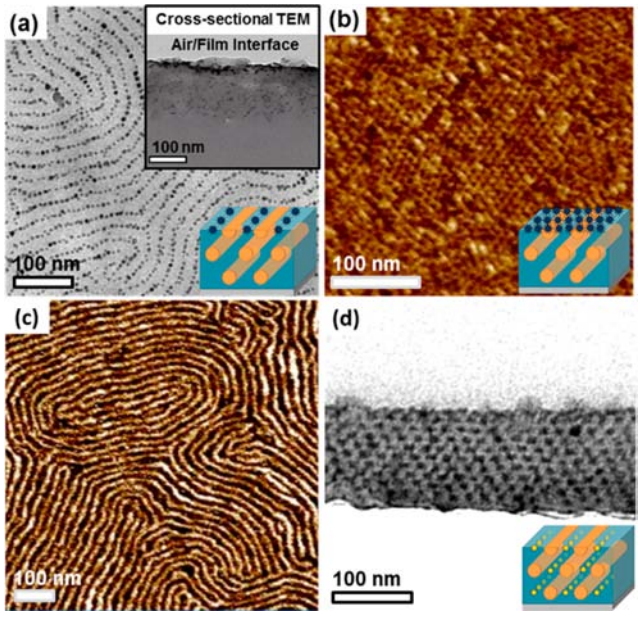

Figure 1. (a) Top-view and cross-sectional (inset) TEM images of a ∼180 nm thin film of PS(19 kDa)-*b*-P4VP(5.6 kDa)(PDP)$_{1.7}$ containing 9.3 nm PbS NPs at $f = 10$ vol %. (b) AFM image showing 2D arrays of 9.3 nm NPs formed at the air/polymer interface when $f = 20$ vol %. (c) AFM and (d) cross-sectional TEM images of a similar film containing 7.4 nm PbS NPs at $f = 10$ vol %, showing hexagonally packed interstitial 3D NP chains parallel to the surface.

pattern of the cylindrical supramolecular morphology. When the NP loading (f) was increased to 20 vol %, the 9.3 nm PbS NPs formed multiple grains of 2D NP hexagonal-close-packed lattices on the film surface, as shown in the atomic force microscopy (AFM) image in Figure 1b. This is in contrast to thin films of supramolecular nanocomposites where the NP size is comparable to the size of the interstitial sites.[28] As shown in Figure 1c,d for comparison, the 7.4 nm PbS NPs were preferentially located in the interstitial area to form 3D NP arrays, and no surface aggregation of the NPs was seen. Positioning the 7.4 nm NPs in the interstitial regions relaxed the supramolecular comb chains from stretching into the interstitial sites, leading to an increase in S_{con} and $S_{geometric}$.[28]

When the NPs are larger than the interstitial sites, it becomes more energetically favorable to expel the NPs to the surface to avoid the entropic penalty (ΔS_{con}) and maximize the enthalpic gain from covering the surface with a layer of NPs that have lower surface tension ($\Delta H_{ligand/air}$). At lower loading, the NPs are preferentially located on top of parallel P4VP(PDP)$_{1.7}$ cylinders at the air/polymer interface because of favorable ligand−polymer interactions, forming single 1D NP chains. As the particle loading increases, localizing the NPs that are much larger than the interstitial sites requires compression of the comb blocks, which is entropically unfavorable. Thus, the NPs cover the entire film surface and form 2D lattices of NPs that lower the surface tension of the film, similar to those observed at the air/liquid interface and in thin films of NP/polymer blends.[33] In thin films of supramolecular nanocomposites, the NPs are expelled to the surface when $d/a \geq 0.28$. This threshold appears to be lower than that for the NP/BCP blend ($d/a \geq 0.3$) and may be indicative of the rigidity of the comb blocks.

When the NP size was reduced to 5.7 nm, different NP assemblies were observed. At $d/a = 0.17$, the 5.7 nm Au NPs

dx.doi.org/10.1021/ja3107912 | J. Am. Chem. Soc. 2013, 135, 1680−1683

were not only segregated into the interstitial regions but also dispersed in the P4VP(PDP)$_{1.7}$ matrix. At f = 3 vol %, most of the 5.7 nm Au NPs were observed to be either localized at the interstitial sites, similar to the 7.4 nm NPs, or dispersed in the cylindrical P4VP(PDP)$_{1.7}$ matrix (Figure 2a). In the P4VP-(PDP)$_{1.7}$ matrix, the 5.7 nm NPs were not homogeneously distributed and formed a lamellar-like morphology with a tilt angle of approximately ±55° relative to the substrate (Figure 2a). At f = 6 vol %, the NPs formed connected and distorted rectangular 3D networks (Figure 2b). We speculate that once the NPs are dispersed in the cylindrical matrix, they disrupt the molecular packing of the P4VP(PDP) comb block, lowering the chain rigidity and entropy associated with chain deformation. This effectively lowers the activation barrier for additional NPs to be solubilized into the region, resulting in the packing of the NPs in a particular direction with respect to the substrate. As f increases, the entire P4VP(PDP)$_{1.7}$ matrix becomes occupied and the NPs are uniformly distributed in the middle of the comb blocks, leading to the formation of a distorted rectangular 3D network of NPs in thin films to maximize S_{trans}.

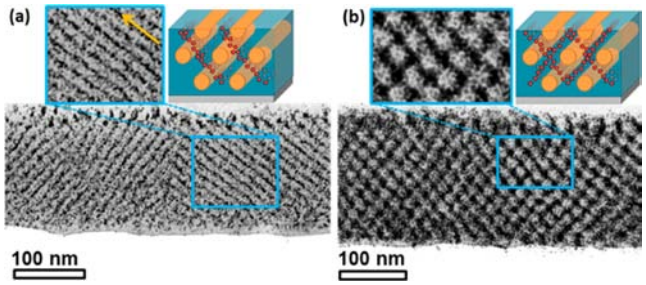

Figure 2. Cross-sectional TEM images of ∼180 nm thin films of PS(19 kDa)-*b*-P4VP(5.6 kDa)(PDP)$_{1.7}$ containing 5.7 nm Au NPs at (a) f = 3 vol % and (b) f = 6 vol %. The 5.7 nm NPs were segregated into the interstitial sites and occupied the entire cylindrical matrix, forming a 3D NP network in the thin film as f increased.

These results show that the entropic contributions to the coassemblies of NPs and cylindrical supramolecules in thin films can be tuned using NPs of different sizes. This allows us to precisely control the spatial organizations of not only a single kind but also two different species of inorganic NPs independently, opening opportunities to obtain 2D and 3D NP assemblies in thin films. Figure 3 shows AFM and cross-sectional TEM images of a ∼200 nm thin film of a nanocomposite containing 7.4 nm Au NPs at f_{Au} = 5 vol % and 9.0 nm PbSe NPs at f_{PbSe} = 15 vol %. The 9.0 nm PbSe NPs formed hexagonally packed 2D NP arrays at the air/polymer interface (Figure 3a), while the 7.4 nm Au NPs formed 3D NP arrays inside the film (Figure 3b). Similarly, a mixture of the 5.7 nm Au NPs and the 9.0 nm PbSe NPs could be coassembled in thin films (Figure 4). Again, the 9.0 nm PbSe NPs formed 2D NP arrays at the air/polymer interface, and the Au NPs were sequestered in the middle of the P4VP(PDP)$_{1.7}$ matrix, forming a distorted rectangular 3D network of NPs. Au NPs first occupy the interstitial sites in the interior of the film, as shown in the region where the NP loading is lower (Figure 4b). Thus, the observed morphologies are essentially superpositions of NP assemblies based on the individual types of NPs.

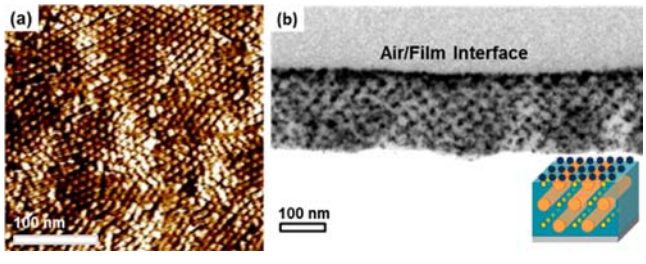

Figure 3. (a) AFM and (b) cross-sectional TEM images of a ∼200 nm thin film of PS(19 kDa)-*b*-P4VP(5.6 kDa)(PDP)$_{1.7}$ containing 7.4 nm Au NPs at 5 vol % and 9.0 nm PbSe NPs at 15 vol %. The hybrid arrays of NPs are composed of a 2D lattice of the 9.3 nm PbS NPs on the surface and a 3D hexagonal lattice of the 7.4 nm Au NPs chains in the interior of the film.

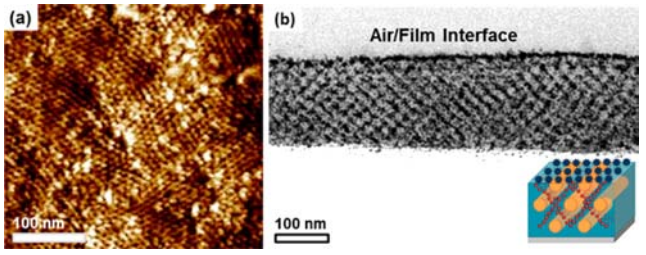

Figure 4. (a) AFM and (b) cross-sectional TEM images of a ∼200 nm thin film of PS(19 kDa)-*b*-P4VP(5.6 kDa)(PDP)$_{1.7}$ containing 5.7 nm Au NPs at 5 vol % and 9.0 nm PbSe NPs at 15 vol %. The morphology is a superposition of those for the 5.7 nm Au and 9.3 nm PbS NP assemblies.

Similar results were observed in the nanocomposite thin films containing both 7.4 nm Au NPs and 5.5 nm PbS NPs (Figure 5). All of the NPs were sequestered in the film interior, and no surface aggregation of NP was observed. When f_{Au} = f_{PbS} = 5 vol %, NPs preferentially filled up the interstitial regions (Figure 5a). Once the interstitial sites are occupied, the 5.5 nm NPs should mainly be distributed in the matrix. On the basis of the experimental results and a qualitative understanding of the thermodynamics of the supramolecular nanocomposite thin films, it is reasonable to speculate that the 7.4 nm NPs should preferentially occupy the interstitial sites. The zoomed-in TEM image in Figure 5a supports this hypothesis. This could lead to hierarchical assemblies of two different particles with

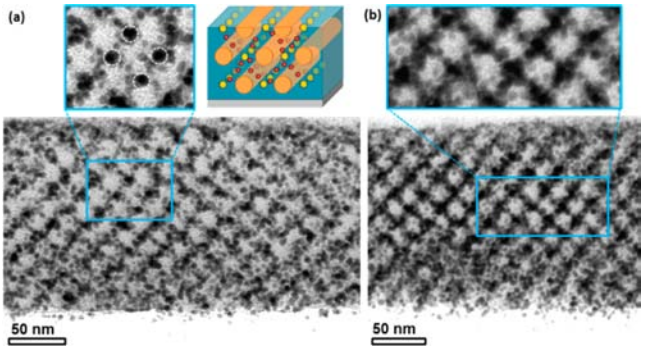

Figure 5. Cross-sectional TEM images of ∼200 nm thin films of PS(19 kDa)-*b*-P4VP(5.6 kDa)(PDP)$_{1.7}$ containing 7.4 nm Au NPs at f_{Au} = 5 vol % and 5.5 nm PbS NPs at (a) f_{PbS} = 5 vol % and (b) f_{PbS} = 10 vol %. The Au and PbS NPs were predominantly located in the interstitial sites, and the smaller PbS NPs began to occupy the entire P4VP(PDP)$_{1.7}$ matrix as f_{PbS} increased from 5 to 10 vol %.

dx.doi.org/10.1021/ja3107912 | *J. Am. Chem. Soc.* 2013, 135, 1680−1683

high spatial precision. Energy-dispersive X-ray analysis (EDX) was used to map the NP spatial distribution but could confirm only the presence of both Au and PbS NPs in the thin films (see the SI) because of the low signal. In the zoomed-in image in Figure 5a, the NPs in the interstitial sites (the NPs in the white circles) appear to be larger than the ones dispersed in the matrix. When f_{PbS} was increased to 10 vol % with f_{Au} fixed at 5 vol %, there were more NPs (presumably the smaller NPs) in the P4VP(PDP)$_{1.7}$ matrix that formed a distorted rectangular 3D network of NPs (Figure 5b). While the present studies showed some promise, further optimization of the NP size distribution is needed to improve the selectivity in order to obtain ideal assemblies as shown schematically in Figure 5. Furthermore, we see a great need to perform theoretical studies to provide useful guidance.

In summary, we have conducted a systematic study on the effect of NP size (d/a ratio) on NP assemblies in thin films of cylindrical nanocomposites and assessed the entropic contribution to the phase behavior of cylindrical nanocomposites in thin films. The observations suggest that the rigid comb blocks in the BCP-based supramolecules are sensitive to the chain deformation upon NP incorporation, allowing us to generate 1D chains, 2D lattices, and 3D arrays and networks of NPs in thin films regardless of the chemical composition of the NPs. This gives us a useful tool for achieving coassemblies of NP mixtures with controlled spatial organization of the hybrid arrays of NPs in thin films, which may provide a platform for systematic investigations of their unique physical properties for plasmonic, energy storage, energy harvesting, electronic, and memory storage devices.

■ ASSOCIATED CONTENT

Supporting Information

Experimental methods; TEM images and size analyses of the PbS, Au, and PbSe NPs used for the thin films; and EDX data confirming the presence of both PbS and Au in the thin film shown in Figure 5b. This material is available free of charge via the Internet at http://pubs.acs.org.

■ AUTHOR INFORMATION

Corresponding Author

tingxu@berkeley.edu

Author Contributions

[⊥]J.K. and P.B. contributed equally.

Notes

The authors declare no competing financial interest.

■ ACKNOWLEDGMENTS

The authors thank Dr. Peter Ercius for collecting the EDX data. This work was supported by the National Science Foundation under Contract DMR-1007002 (J.K. and T.X.) and by the Department of Energy, Office of Basic Energy Sciences, under Contract DE-AC02-05CH11231 (P.B., J.M.L., A.P.A., and T.X.).

■ REFERENCES

(1) Redl, F. X.; Cho, K. S.; Murray, C. B.; O'Brien, S. *Nature* **2003**, *423*, 968.
(2) Talapin, D. V.; Murray, C. B. *Science* **2005**, *310*, 86.
(3) Urban, J. J.; Talapin, D. V.; Shevchenko, E. V.; Kagan, C. R.; Murray, C. B. *Nat. Mater.* **2007**, *6*, 115.
(4) Chen, J.; Dong, A.; Cai, J.; Ye, X.; Kang, Y.; Kikkawa, J. M.; Murray, C. B. *Nano Lett.* **2010**, *10*, 5103.
(5) Kulakovich, O.; Strekal, N.; Yaroshevich, A.; Maskevich, S.; Gaponenko, S.; Nabiev, I.; Woggon, U.; Artemyev, M. *Nano Lett.* **2002**, *2*, 1449.
(6) Govorov, A. O.; Bryant, G. W.; Zhang, W.; Skeini, T.; Lee, J.; Kotov, N. A.; Slocik, J. M.; Naik, R. R. *Nano Lett.* **2006**, *6*, 984.
(7) Ito, Y.; Matsuda, K.; Kanemitsu, Y. *Phys. Rev. B* **2007**, *75*, No. 033309.
(8) Akimov, A. V.; Mukherjee, A.; Yu, C. L.; Chang, D. E.; Zibrov, A. S.; Hemmer, P. R.; Park, H.; Lukin, M. D. *Nature* **2007**, *450*, 402.
(9) Fedutik, Y.; Temnov, V. V.; Schops, O.; Woggon, U.; Artemyev, M. V. *Phys. Rev. Lett.* **2007**, *99*, No. 136802.
(10) Shevchenko, E. V.; Ringler, M.; Schwemer, A.; Talapin, D. V.; Klar, T. A.; Rogach, A. L.; Feldmann, J.; Alivisatos, A. P. *J. Am. Chem. Soc.* **2008**, *130*, 3274.
(11) Parthasarathy, R.; Lin, X.-M.; Jaeger, H. M. *Phys. Rev. Lett.* **2001**, *87*, No. 186807.
(12) Tran, T. B.; Beloborodov, I. S.; Lin, X. M.; Bigioni, T. P.; Vinokur, V. M.; Jaeger, H. M. *Phys. Rev. Lett.* **2005**, *95*, No. 076806.
(13) Talapin, D. V.; Lee, J.-S.; Kovalenko, M. V.; Shevchenko, E. V. *Chem. Rev.* **2010**, *110*, 389.
(14) Bockstaller, M. R.; Mickiewicz, R. A.; Thomas, E. L. *Adv. Mater.* **2005**, *17*, 1331.
(15) Balazs, A. C.; Emrick, T.; Russell, T. P. *Science* **2006**, *314*, 1107.
(16) Kao, J.; Thorkelsson, K.; Bai, P.; Rancatore, B. J.; Xu, T. *Chem. Soc. Rev.* **2012**, DOI: 10.1039/C2CS35375J.
(17) Zhao, Y.; Thorkelsson, K.; Mastroianni, A. J.; Schilling, T.; Luther, J. M.; Rancatore, B. J.; Matsunaga, K.; Jinnai, H.; Wu, Y.; Poulsen, D.; Fréchet, J. M. J.; Alivisatos, A. P.; Xu, T. *Nat. Mater.* **2009**, *8*, 979.
(18) Chiu, J. J.; Kim, B. J.; Kramer, E. J.; Pine, D. J. *J. Am. Chem. Soc.* **2005**, *127*, 5036.
(19) Thompson, R. B.; Ginzburg, V. V.; Matsen, M. W.; Balazs, A. C. *Science* **2001**, *292*, 2469.
(20) Huh, J.; Ginzburg, V. V.; Balazs, A. C. *Macromolecules* **2000**, *33*, 8085.
(21) Lee, J. Y.; Thompson, R. B.; Jasnow, D.; Balazs, A. C. *Macromolecules* **2002**, *35*, 4855.
(22) Bockstaller, M. R.; Lapetnikov, Y.; Margel, S.; Thomas, E. L. *J. Am. Chem. Soc.* **2003**, *125*, 5276.
(23) Lin, Y.; Boker, A.; He, J. B.; Sill, K.; Xiang, H. Q.; Abetz, C.; Li, X. F.; Wang, J.; Emrick, T.; Long, S.; Wang, Q.; Balazs, A.; Russell, T. P. *Nature* **2005**, *434*, 55.
(24) Gupta, S.; Zhang, Q.; Emrick, T.; Balazs, A. C.; Russell, T. P. *Nat. Mater.* **2006**, *5*, 229.
(25) Li, Q.; He, J.; Glogowski, E.; Li, X.; Wang, J.; Emrick, T.; Russell, T. P. *Adv. Mater.* **2008**, *20*, 1462.
(26) Meli, L.; Arceo, A.; Green, P. F. *Soft Matter* **2009**, *5*, 533.
(27) Kim, J.; Green, P. F. *Macromolecules* **2010**, *43*, 1524.
(28) Kao, J.; Bai, P.; Chuang, V. P.; Jiang, Z.; Ercius, P.; Xu, T. *Nano Lett.* **2012**, *12*, 2610.
(29) Jang, S. G.; Khan, A.; Hawker, C. J.; Kramer, E. J. *Macromolecules* **2012**, *45*, 1553.
(30) Wang, Q.; Nealey, P. F.; de Pablo, J. J. *J. Chem. Phys.* **2003**, *118*, 11278.
(31) Shull, K. R.; Winey, K. I. *Macromolecules* **1992**, *25*, 2637.
(32) Shull, K. R.; Mayes, A. M.; Russell, T. P. *Macromolecules* **1993**, *26*, 3929.
(33) Bigioni, T. P.; Lin, X.-M.; Nguyen, T. T.; Corwin, E. I.; Witten, T. A.; Jaeger, H. M. *Nat. Mater.* **2006**, *5*, 265.